

1 **Increased Importance of Aerosol-Cloud Interaction for Surface**
2 **PM_{2.5} Pollution Relative to Aerosol-Radiation Interaction in**
3 **China with the Anthropogenic Emission Reduction**

4
5 Da Gao^{1, 2}, Bin Zhao^{1, 2, *}, Shuxiao Wang^{1, 2}, Yuan Wang³, Brian Gaudet⁴, Yun
6 Zhu⁵, Xiaochun Wang^{1, 2}, Jiewen Shen^{1, 2}, Shengyue Li^{1, 2}, Yicong He^{1, 2}, Dejia
7 Yin^{1, 2}, Zhaoxin Dong^{1, 2}

8
9 ¹State Key Joint Laboratory of Environment Simulation and Pollution Control,
10 School of Environment, Tsinghua University, 100084 Beijing, China

11 ²State Environmental Protection Key Laboratory of Sources and Control of Air
12 Pollution Complex, Beijing, 100084, China

13 ³Department of Earth, Atmospheric, and Planetary Sciences, Purdue University,
14 West Lafayette, IN, USA,

15 ⁴Pacific Northwest National Laboratory, Richland, Washington, USA

16 ⁵Guangdong Provincial Key Laboratory of Atmospheric Environment and
17 Pollution Control, College of Environment and Energy, South China University
18 of Technology, Guangzhou Higher Education Mega Center, Guangzhou, 510006,
19 China

20 *Correspondence to: Bin Zhao (bzhao@mail.tsinghua.edu.cn)

21
22 **Abstract:** Surface fine particulate matter (PM_{2.5}) pollution can be enhanced by

23 feedback processes induced by aerosol-radiation interactions (ARI) and aerosol-
24 cloud interactions (ACI). Many previous studies have reported enhanced PM_{2.5}
25 concentration induced by ARI and ACI for episodic events in China. However,
26 few studies have examined the changes in the ARI- and ACI-induced PM_{2.5}
27 enhancements over a long period, though the anthropogenic emissions have
28 changed substantially in the last decade. In this study, we quantify the ARI- and
29 ACI-induced PM_{2.5} changes for 2013–2021 under different meteorology and
30 emission scenarios using the Weather Research and Forecasting model with
31 Chemistry (WRF-Chem) and investigate the driving factors for the changes. Our
32 results show that in January 2013, when China suffered from the worst PM_{2.5}
33 pollution, the PM_{2.5} enhancement induced by ARI in eastern China (5.59 μg m⁻³)
34 is larger than that induced by ACI (3.96 μg m⁻³). However, the ACI-induced
35 PM_{2.5} enhancement shows a significantly smaller decrease ratio (51%) than the
36 ARI-induced enhancement (75%) for 2013–2021, making ACI more important
37 for enhancing PM_{2.5} concentrations in January 2021. Our analyses suggest that
38 the anthropogenic emission reduction plays a key role in this shift. Owing to only
39 anthropogenic emission reduction, the ACI-induced PM_{2.5} enhancement
40 decreases by 43% in January, lower than the decrease ratio of the ARI-induced
41 enhancement (57%). The relative change in ARI- and ACI-induced PM_{2.5}
42 enhancement in July is similar to the pattern observed in January caused by
43 anthropogenic emission reduction. The primary reason for this phenomenon is
44 that the decrease of ambient PM_{2.5} for 2013–2021 causes a disproportionately

45 small decrease of liquid water path (LWP) and increase of cloud effective radius
46 (Re) under the condition of high PM_{2.5} concentration. Therefore, the surface solar
47 radiation attenuation (and hence boundary layer height reduction) caused by ACI
48 decreases slower than that caused by ARI. Moreover, the lower decrease ratio of
49 the ACI-induced PM_{2.5} enhancement is dominated by the lower decrease ratio of
50 ACI-induced secondary PM_{2.5} component enhancement, which is additionally
51 caused by smaller decrease ratio of the air temperature reduction and relative
52 humidity (RH) increase. Our findings indicate that, with the decrease of ambient
53 PM_{2.5}, the ACI-induced PM_{2.5} enhancement inevitably becomes more important.
54 This needs to be considered in the formulation of control policies to meet the
55 national PM_{2.5} air quality standard.

56

57 **1. Introduction**

58 Aerosol-radiation interaction (ARI) and aerosol-cloud interaction (ACI) are
59 important ways for aerosols to influence the climate (Rosenfeld et al., 2014;
60 Seinfeld et al., 2016; Liu et al., 2018; Bellouin et al., 2020; Forster et al., 2021).
61 The ARI represents the direct scattering and absorption of solar and infrared
62 radiation by atmospheric aerosols; the ACI denotes the modification effects on
63 the lifetime, physical and optical properties of clouds by atmospheric aerosols.

64 Previous studies have documented that both ARI and ACI have important
65 contributions to inhibiting the planetary boundary layer height (PBLH), cooling
66 the near-surface air temperature, and increasing the relative humidity (RH) (Wang
67 et al., 2014; Ding et al., 2016; Liu et al., 2018). Moreover, ACI has extra

68 contributions to changing precipitation and cloud chemistry (Zhao et al., 2017;
69 Zhang et al., 2018). These feedbacks and changes are mostly conducive to
70 increasing the haze severity (Wang et al., 2015; Zhang et al., 2018; Liu et al.,
71 2018; Zhou et al., 2019; Zhang et al., 2020; Xiong et al., 2022; Lin et al., 2022).
72 So far, numerous studies have evaluated the fine particulate matter (PM_{2.5})
73 enhancements caused by the decreases of downward shortwave radiation at the
74 surface (SWDOWN), PBLH, near-surface air temperature and precipitation, and
75 by the increase of RH, especially during the severe PM_{2.5} pollution in China (Le
76 et al., 2020). Zhang et al. (2015) and Zhang et al. (2018) quantified that the ARI
77 caused the PM_{2.5} increase by 8.3 $\mu\text{g m}^{-3}$ in 2013 and 4.0 $\mu\text{g m}^{-3}$ in 2014. However,
78 both positive and negative contributions of ACI to the PM_{2.5} have been revealed
79 (Forkel et al., 2012; 2015; Kong et al., 2015; Zhang et al., 2015; Zhang et al.,
80 2018). Zhao et al. (2017) pointed out that the negative contribution of ACI shown
81 in some studies (Gustafson et al., 2007; Gong et al., 2015) is due to the relatively
82 high prescribed values of cloud droplet number concentration (CDNC) or cloud
83 condensation nuclei (CCN), which could not represent a rather clean condition.
84 Besides, there might be a discrepancy between the enhancements induced by ARI
85 and ACI for primary and secondary PM_{2.5} components. The primary PM_{2.5}
86 components are mainly influenced by physical transport, while the secondary
87 PM_{2.5} components are also affected by chemical formation and decomposition.
88 The lower air temperature and higher RH can help to condense gas precursors
89 into secondary aerosol particles (Donahue et al., 2012) and strengthen aqueous

90 and heterogeneous reactions (Liu et al., 2018). On the contrary, Wu et al. (2020)
91 pointed out that the ARI may also suppress the formation of secondary aerosol
92 because the atmospheric oxidizing capacity and photolysis rate can be changed
93 during the scattering and absorbing of solar radiation. Therefore, not all changes
94 of meteorological factors are conducive to the increase of secondary PM_{2.5}, and
95 these positive and negative contributions would influence the variations of
96 primary and secondary PM_{2.5} components. In a word, although the ARI and ACI
97 processes mostly lead to a net PM_{2.5} increase, the relative increasing rates of
98 different aerosol components are fairly complex due to various physical and
99 chemical processes.

100 In recent years, the Chinese government has successively proclaimed the
101 policies of “Air pollution prevention and control action plan” and “Three-year
102 action plan to win the blue sky defense war”, including the promotion of ultra-
103 low emission technologies in industrial sectors, the implementation of traffic
104 restriction policies, and the transition from coal to gas in residential cooking. As
105 a result, the annually averaged PM_{2.5} concentrations in Beijing-Tianjin-Hebei
106 region, Yangtze River Delta (YRD) and Pearl River Delta have been reduced by
107 39.6%, 34.2%, and 27.7% from 2013 to 2017, respectively (Wang et al., 2017;
108 Ding et al., 2019a). Meanwhile, sulfate and organic components have respectively
109 decreased by 76% and 70 % in the North China Plain (NCP) (Wang et al., 2019).
110 Considering the sharp anthropogenic emission reduction and PM_{2.5} concentration
111 decrease, Moch et al. (2022) found that the decrease in mean PM_{2.5} concentration

112 from the winter months of 2012–2013 to the winter months of 2016–2017 in
113 China weakened the cloud–snowfall–albedo feedback induced by the aerosol
114 semi-direct effect. For air quality, Zhang et al. (2022) found that the decrease in
115 black carbon from 2013 to 2017 in China reduced the enhanced $PM_{2.5}$
116 concentration induced by the ARI by $1.8 \mu\text{g m}^{-3}$ in January and $0.3 \mu\text{g m}^{-3}$ in
117 July.

118 However, none of the previous studies have systematically evaluated the
119 changes in enhanced $PM_{2.5}$ concentrations through ARI and ACI in China at the
120 long-term scale. Besides, the driving force and physical mechanisms for the
121 changes are also yet to be explored. In this study, we try to investigate the
122 enhanced $PM_{2.5}$ concentrations induced by ARI and ACI in 2013 over China, the
123 impact of the changes in the meteorological background and anthropogenic
124 emission from 2013 to 2021 on ARI- and ACI-induced $PM_{2.5}$ enhancements and
125 its components. Furthermore, the causes of $PM_{2.5}$ enhancement changes are
126 analyzed.

127

128 **2. Model and experimental design**

129 **2.1 Model configuration**

130 The Weather Research and Forecasting model with Chemistry (WRF-Chem)
131 version 4.2 has been used in this study. The model domain covers the whole land
132 area of China with a horizontal resolution of $27 \text{ km} \times 27 \text{ km}$. There are 24 vertical
133 layers from surface to 50 hPa, with denser layers in the planetary boundary layer

134 (PBL). Major physical options used in the model include the Morrison double-
135 moment scheme (Morrison et al., 2009), the Rapid Radiative Transfer Model for
136 GCMs (RRTMG) shortwave and longwave radiative transfer schemes (Iacono et
137 al., 2008), the Eta similarity surface-layer scheme (Janjic et al., 1994), the Noah
138 land-surface model with multiple parameterization options (Niu et al., 2011), the
139 Bougeault and Lacarrere PBL scheme (Bougeault et al., 1989), and the Grell-
140 Freitas ensemble cumulus scheme (Grell et al., 2014). For chemistry, we employ
141 the SAPRC-99 (Statewide Air Pollution Research Center mechanism, version
142 1999) as the gas-phase chemistry mechanism (Carter et al., 2000). The aerosol
143 module used in the study is the Model for Simulating Aerosol Interactions and
144 Chemistry (MOSAIC) (Zaveri et al., 2008), which includes all major aerosol
145 processes and represents the aerosol size distribution with 8 size bins. The
146 MOSAIC also incorporates the one-dimensional Volatility Basis Set (VBS)
147 framework that improves the simulation of secondary organic aerosol
148 (Shrivastava et al., 2011). Rates for photolytic reactions are calculated using the
149 Fast-J photolysis rate scheme (Wild et al., 2000). Additionally, we noted the poor
150 ability of nitrate simulation in the WRF-Chem model. We improved the nitrate
151 simulation by addressing the HONO underestimation in the model (Wang et al.,
152 2015; Xue et al., 2020). More detailed information can be found in Section 1 in
153 the Supplementary Information. The meteorological initial and boundary
154 conditions are derived from the National Centers for Environmental Prediction
155 Final Analysis reanalysis data with resolutions of $1.0^\circ \times 1.0^\circ$ and 6 h

156 (<http://rda.ucar.edu/datasets/ds083.2/>). The chemical initial and boundary
157 conditions are acquired from the simulation results of the National Center for
158 Atmospheric Research's Community Atmosphere Model with Chemistry (CAM-
159 Chem, before 2020, <https://www.acom.ucar.edu/cam-chem/cam-chem.shtml>) and
160 the Whole Atmosphere Community Climate Model (WACCM, after 2020,
161 <https://www.acom.ucar.edu/waccm/download.shtml>) with resolutions of $0.94^\circ \times$
162 1.25° and 6 h.

163 The anthropogenic emission data in China for 2013-2021 are obtained from
164 the ABaCAS-EI (Air Benefit and Cost and Attainment Assessment System-
165 Emission Inventory) developed by Tsinghua University (Li et al., 2023). Specific
166 emissions of SO_2 , NO_x (NO and NO_2), NH_3 , $\text{PM}_{2.5}$ and VOCs in 2013 and 2021
167 are presented in Table S2. The emission data in other countries are obtained from
168 the IIASA emission inventory for 2015 (Zheng et al., 2019; Gao et al., 2020). The
169 biogenic emission is calculated online by the Model of Emissions of Gases and
170 Aerosols from Nature (MEGAN) v2.04 (Guenther et al., 2006). The dust emission
171 is calculated online by the Goddard Chemistry Aerosol Radiation and Transport
172 (GOCART) model coupled with the MOSAIC aerosol schemes. (Zhao et al., 2010;
173 2013)

174 To account for the physical processes of aerosol-radiation-cloud feedback
175 on meteorological factors and $\text{PM}_{2.5}$, the four-dimensional data assimilation
176 (FDDA) is not utilized in our simulations. Aerosol optical depth, single scattering
177 albedo, and asymmetry factors are calculated based on the Lorenz-Mie theory as

178 a function of wavelength and three-dimensional location (Fast et al., 2006). Then,
179 the aerosol optical properties are transferred to the RRTMG radiation scheme to
180 calculate the impact of aerosol on the radiation balance (Iacono et al., 2008). As
181 for the ACI, activated aerosols are calculated by the Abdul-Razzak and Ghan
182 scheme (Abdul-Razzak & Ghan, 2002) and are then coupled with the Morrison
183 two-moment cloud microphysics scheme (Morrison et al., 2009). The prognostic
184 cloud water content calculated by the Morrison scheme is input into the RRTMG
185 scheme for the radiative transfer calculation. It should be noted that the prognostic
186 aerosol does not influence cumulus clouds and ice nucleation in the model. The
187 prognostic aerosol can only be activated as CCN. It does not directly contribute
188 to ice nucleation, which is only influenced by air temperature and supersaturation
189 (Kanji et al., 2017). Furthermore, CCN would influence grid-scale clouds.
190 However, limited by the horizontal resolution of $27 \text{ km} \times 27 \text{ km}$, cumulus clouds
191 could not be resolved in this grid.

192

193 **2.2 Experimental design**

194 As described in the introduction, the purpose of this study is to quantify the
195 contributions of ARI and ACI to $\text{PM}_{2.5}$ concentrations under different emission
196 scenarios. The simulation periods are January and July, 2013 and 2021,
197 representing winter and summer, respectively.

198 As shown in Table 1, the enhanced $\text{PM}_{2.5}$ concentration induced by ARI and
199 ACI could be obtained via comparing the simulation results with ARI or ACI

200 turned on or off. By setting the ‘aer_ra_feedback’ to 0 in the model, the ARI could
 201 be turned off, which means that the interaction between aerosol and radiation is
 202 prevented. The ACI could be turned off through prescribing the CDNC of 25 cm^{-3}
 203 in the microphysical scheme, which represents average level in the pristine air
 204 (Bennartz et al., 2007). For example, the 13M13E_B, 13M13E_NR and
 205 13M13E_NRC shown in Table 1 represent the cases with ARI and ACI effects,
 206 without ARI effect, and without ARI and ACI effects in 2013, respectively. The
 207 ARI-induced $\text{PM}_{2.5}$ enhancement could be acquired by comparing the results of
 208 13M13E_B and 13M13E_NR; the ACI-induced $\text{PM}_{2.5}$ enhancement could be
 209 obtained by comparing the results of 13M13E_NR and 13M13E_NRC.

210

211 **Table 1. Case definition under different meteorological backgrounds and**
 212 **anthropogenic emissions with ARI or ACI turned on or off.**

Case	Meteorology	Emission	ARI	ACI
13M13E_B	Jan & Jul, 2013	Jan & Jul, 2013	on	on
13M13E_NR	Jan & Jul, 2013	Jan & Jul, 2013	off	on
13M13E_NRC	Jan & Jul, 2013	Jan & Jul, 2013	off	off
21M13E_B	Jan & Jul, 2021	Jan & Jul, 2013	on	on
21M13E_NR	Jan & Jul, 2021	Jan & Jul, 2013	off	on
21M13E_NRC	Jan & Jul, 2021	Jan & Jul, 2013	off	off
21M21E_B	Jan & Jul, 2021	Jan & Jul, 2021	on	on
21M21E_NR	Jan & Jul, 2021	Jan & Jul, 2021	off	on

213

214 In order to obtain the changes of the ARI- and ACI-induced $PM_{2.5}$
 215 enhancements from 2013 to 2021 caused by the variation of meteorological
 216 background and by the reduction of anthropogenic emission, the control
 217 experiments (21M13E; three experiments: with ARI and ACI turned on, with ARI
 218 turned off and ACI turned on, and with ARI and ACI turned off) are designed
 219 with the meteorological background in 2021 and the anthropogenic emission in
 220 2013. In the following, the 13M13E, 21M13E and 21M21E represent the cases
 221 with meteorological background and anthropogenic emission in 2013,
 222 meteorological background in 2021 and anthropogenic emission in 2013, and
 223 meteorological background and anthropogenic emission in 2021, respectively.
 224 Taking the ARI for example, the change of the ARI-induced $PM_{2.5}$ enhancement
 225 from the variation of meteorological background is obtained by subtracting the
 226 ARI-induced $PM_{2.5}$ enhancement in the 13M13E from that in the 21M13E [Eq.
 227 (1)]; the change in the ARI-induced $PM_{2.5}$ enhancement from the reduction of
 228 anthropogenic emission is obtained by subtracting the ARI-induced $PM_{2.5}$
 229 enhancement in the 21M13E from that in the 21M21E [Eq. (2)]. The calculations
 230 for the ACI-induced $PM_{2.5}$ enhancement are similar, as shown in Eqs. (3) and (4).

231

$$ARI_{met} = (21M13E_B - 21M13E_{NR}) - (13M13E_B - 13M13E_{NR}), \quad (1)$$

$$ARI_{emi} = (21M21E_B - 21M21E_NR) - (21M13E_B - 21M13E_NR), \quad (2)$$

$$ACI_{met} = (21M13E_NR - 21M13E_NRC) - (13M13E_NR - 13M13E_NRC), \quad (3)$$

$$ACI_{emi} = (21M21E_NR - 21M21E_NRC) - (21M13E_{NR} - 21M13E_{NRC}), \quad (4)$$

232 where the ARI_{met} (ACI_{met}) and ARI_{emi} (ACI_{emi}) represent the changes of the
 233 enhanced $PM_{2.5}$ concentration induced by the ARI (ACI) from 2013 to 2021
 234 caused by the variation of meteorological background and reduction of
 235 anthropogenic emission, respectively.

236

237 **2.3 Model evaluation**

238 To determine the accuracy and reliability of simulation results, the
 239 13M13E_B and 21M21E_B simulations (Table 1) are verified by using the
 240 observations. The variables checked in the evaluation contain the concentration
 241 and components of surface $PM_{2.5}$ and the meteorological factors, including air
 242 temperature (T2) and water vapor mixing ratio (Q2) at 2 m, wind speed (WS10)
 243 and wind direction (WD10) at 10 m, as well as cloud fraction (CF) and liquid
 244 water path (LWP).

245 Simulated temperature, wind, and water vapor are compared with the
 246 observations from the National Climate Data Center (NCDC,
 247 <http://www.ncdc.noaa.gov/>). The evaluation shows that the absolute errors for T2,

248 WS10 and Q2 are respectively less than 1°C , 1 m s^{-1} and 0.1 g kg^{-1} (Table S3),
249 and those for WD10 are near or less than 10° . For the simulation utilizing the
250 FDDA, the benchmarks of biases proposed by Emery et al. (2001) are 0.7°C , 0.6
251 m s^{-1} , 1.0 g kg^{-1} and 20° for the T2, WS10, Q2 and WD10, respectively. The
252 biases of the T2 and WS10 in our simulations have exceeded the benchmarks,
253 while they are still similar to or smaller than in most previous WRF-Chem
254 applications without FDDA over East Asia (Zhang et al., 2015; Zhao et al., 2017).

255 Simulated CF and LWP are compared with the data from the Moderate-
256 resolution Imaging Spectroradiometer (MODIS) aboard the Terra satellite
257 (<http://ladsweb.nascom.nasa.gov/data/search.html>). Overall, the CF and LWP
258 simulations are in good agreement with the observations (Figs. S1 and S2). The
259 high values of observed CF and LWP primarily appear in the south of China in
260 January 2013 and 2021, and high value of CF also occurs in the NCP region. The
261 high values of CF and LWP in the south of China could be reproduced in the
262 simulation, while the CF in NCP region is slightly underestimated, which could
263 be owing to imperfect cloud parameterization scheme in the model or
264 uncertainties in the retrieval of MODIS datasets. In July 2013 and 2021, part of
265 high value area of observed LWP and most high value area of observed CF appear
266 in the southwestern China and the east coast of China, which also could be
267 captured by the simulation. In addition, high LWP also appears in Gansu and
268 Sichuan Provinces in July 2013 and in the YRD and Sichuan-Chongqing in July
269 2021, which are both well reproduced. The distributions of low values of

270 observed CF and LWP in January and July of 2013 and 2021 are also well
271 simulated.

272 The simulation of surface PM_{2.5} concentration is compared with the data
273 from the China National Environmental Monitoring Center
274 (<https://quotsoft.net/air/>). The evaluation shows that both the regional average
275 value and spatial distribution of simulated PM_{2.5} concentration are in good
276 agreement with the observational data. As shown in Fig. S3, the biases of regional
277 average PM_{2.5} concentration in January and July of 2013 and 2021 are below 3
278 $\mu\text{g m}^{-3}$ in eastern China. In this study, the eastern China includes most of Chinese
279 provinces except Xinjiang, Xizang, Ningxia, Qinghai, Gansu, Inner-Mongolia
280 and Heilongjiang Provinces, which contains most polluted regions in China. In
281 addition, the distributions of high simulated PM_{2.5} concentration are also
282 consistent with the observations, such as the NCP region, the YRD region, and
283 the Sichuan-Chongqing area.

284 The simulated PM_{2.5} components are also reasonable compared with the
285 observation data. Given that the PM_{2.5} components data in 2013 are very rare, we
286 sourced three sets of data in January 2013, respectively in Beijing (Mattias et al.,
287 2017), Handan (Zhang et al., 2015), and Shanghai (Li et al., 2015). The results
288 show that the simulated PM_{2.5} components are reproduced well generally.
289 Specifically, the simulated PM_{2.5} components are larger than half of observational
290 PM_{2.5} components and less than the double observational PM_{2.5} components (Fig.
291 S4). Observed PM_{2.5} components data in 2021 are from a data sharing platform

292 for the NCP region and its surrounding areas (Wang et al., 2019). Fig. S5 shows
293 the ratios of observation to simulation of ammonium, sulfate, BC and organic
294 carbon (OC) in January and July 2021. The results exhibit that almost all the ratios
295 of PM_{2.5} components are located between 0.5 and 2.0, while some ratios of sulfate
296 in January, part of OC in January, and BC in January and July are beyond this
297 range. But these discrepancies will not cause obvious uncertainties in this
298 research. Specifically, considering BC low hygroscopicity, BC overestimations
299 in January and July 2021 probably bring low uncertainties in ACI-induced PM_{2.5}
300 enhancement. To test the impact of simulated BC overestimation in January 2021
301 on ARI-induced PM_{2.5} enhancement, we utilize another set of particulate matter
302 (PM) source profiles (Liu et al., 2018) and conduct the simulations for January
303 2021. The results indicate that the ratios of simulated BC concentration to
304 observational BC concentration are within 2.0. The ARI-induced PM_{2.5}
305 enhancement is 1.33 $\mu\text{g m}^{-3}$, which shows a negligible difference from the result
306 (1.37 $\mu\text{g m}^{-3}$) obtained using original PM source profiles (Fig. S6). In view of the
307 results in January 2021, the BC overestimation in July 2021 also probably brings
308 low uncertainties in ARI-induced PM_{2.5} enhancement. However, the reduction in
309 simulated BC concentration in January 2021 does not necessarily mean that this
310 set of PM source profiles is better than the original PM source profiles, because
311 this might be an accidental result caused by other uncertainties. For example, the
312 current model underestimates the wet deposition of BC due to neglecting the
313 increase in BC hygroscopicity brought about by BC aging. If this process is

314 considered in the model, simulated BC concentrations might be better reproduced
315 using original PM source profiles. Therefore, in this study, we still use the original
316 results for our analysis. The model also underestimates the sulfate concentration
317 and overestimates the part of OC concentration in January 2021. We think that
318 neither of these discrepancies will cause significant uncertainties in ARI- and
319 ACI-induced PM_{2.5} enhancement. Specifically, the majority of aerosol is
320 scattering aerosol and the PM_{2.5} concentration in January 2021 is reproduced well.
321 Therefore, we think that the impact of the sulfate underestimation on the ARI-
322 induced PM_{2.5} enhancement would be largely offset by the overestimation of
323 other scattering aerosol components, such as OC. In addition, the OC
324 overestimation should not bring significant uncertainty to ACI-induced PM_{2.5}
325 enhancement either, because of the relatively lower hygroscopicity of OC
326 compared to secondary inorganic aerosol. The underestimation of sulfate
327 simulation in January 2021 also minimally affects ACI-induced PM_{2.5}
328 enhancement because the sulfate underestimation mainly occurs in the North
329 China Plain, where cloud cover is low. In contrast, in southern cities such as
330 Mianyang city in Sichuan province where there is plenty of cloud cover, the
331 sulfate simulation was 4.19 $\mu\text{g m}^{-3}$ in January 2021, which is very close to the
332 observed value of 4.25 $\mu\text{g m}^{-3}$ (Lin et al., 2022).

333 In summary, the performances of WRF-Chem model on the simulations of
334 air quality and meteorological factors over China are fairly good, and the
335 differences between simulations and observations are reasonable and acceptable.

336

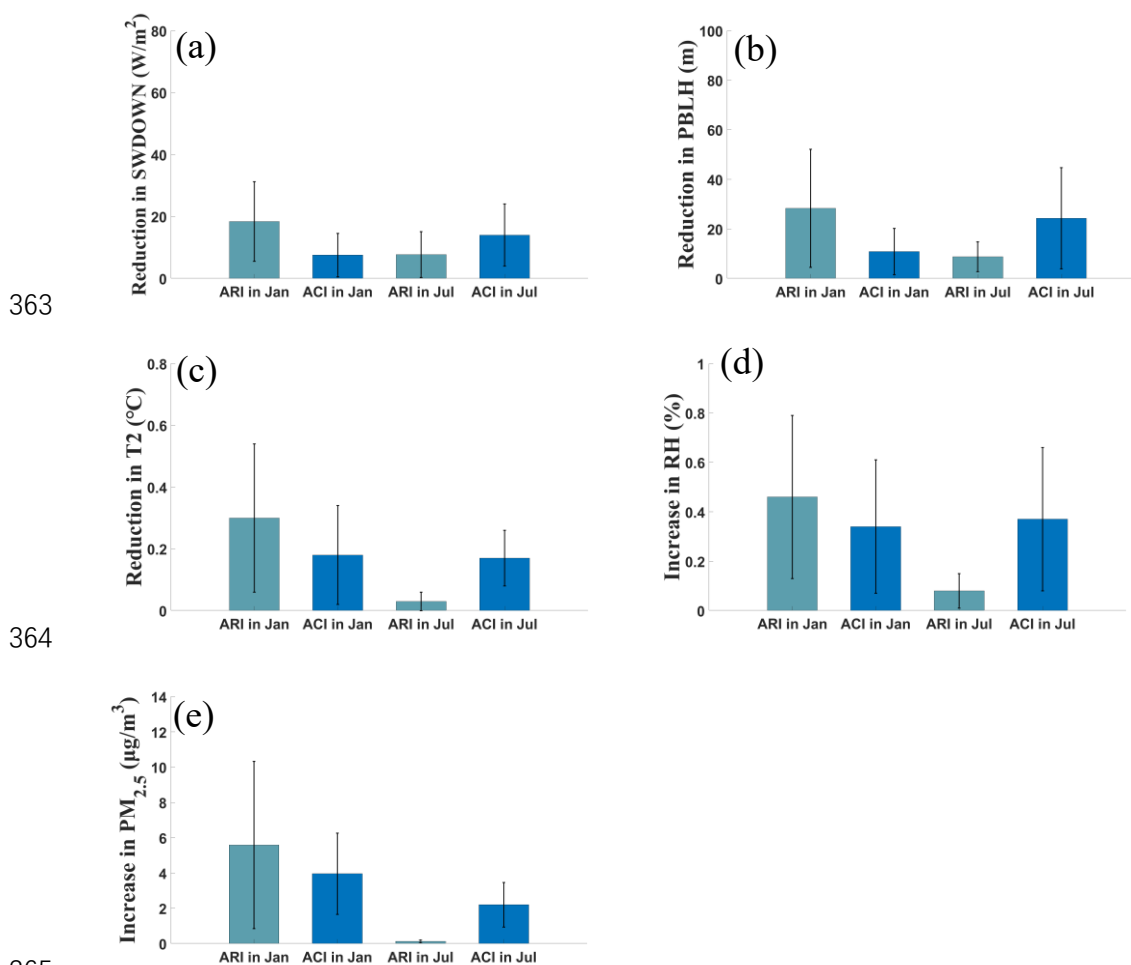
337 **3. Results and discussion**

338 **3.1 The impacts of ARI and ACI feedbacks on the meteorological** 339 **factors and PM_{2.5} concentrations in 2013**

340 We comprehensively discuss the effects of ARI and ACI on the regional
341 meteorological factors and PM_{2.5} concentrations in January and July 2013. Fig. 1
342 shows the impacts of ARI and ACI feedbacks on the SWDOWN, PBLH, T2, RH
343 and PM_{2.5} concentration in January and July 2013. For the ARI, the SWDOWN
344 decreases by 18.37 and 7.71 W m⁻² in January and July 2013 in eastern China,
345 respectively. Since the incoming solar radiation reaching the ground is reduced
346 by PM, the T2 and PBLH in eastern China further decrease by 0.30 and 0.03°C,
347 and 28.34 and 8.75 m in January and July 2013, respectively. Meanwhile, the RH
348 increases by 0.46% and 0.08% due to the water vapor accumulation in the
349 suppressed planetary boundary layer (Liu et al., 2018). Ultimately, the PM_{2.5}
350 concentration increases by 5.59 and 0.13 μg m⁻³ in eastern China (Fig. 1d). For
351 the ACI, affected by the cloud modified by the aerosol, the SWDOWN, T2 and
352 PBLH decrease by 7.54 and 14.03 W m⁻², 0.18 and 0.17 °C, and 10.89 and 24.31
353 m, and the RH increases by 0.34% and 0.37% in January and July 2013 in eastern
354 China, respectively. As a result, the PM_{2.5} concentration increases by 3.96 and
355 2.20 μg m⁻³ in eastern China. Fig. 2 shows that the regional averaged values and
356 spatial distributions of PM_{2.5} enhancements induced by ARI and ACI in 2013 are
357 in line with the results of previous studies (Zhao et al., 2017; Zhang et al., 2018).

358 Overall, the enhanced $PM_{2.5}$ concentration induced by ARI is greater than
 359 that induced by ACI in January 2013, which is due to the relatively low LWP in
 360 the high $PM_{2.5}$ concentration area. But it shows the opposite situation in July 2013,
 361 owing to the plentiful cloud in warm July (Zhang et al., 2018).

362



366 Fig. 1. The regional averaged reductions of (a) downward shortwave radiation at
 367 the surface (SWDOWN), (b) planetary boundary layer height (PBLH), (c) 2-m
 368 air temperature (T2), and increments of (d) relative humidity (RH) and (e) fine
 369 particulate matter ($PM_{2.5}$) concentration induced by the aerosol-radiative
 370 interaction (ARI) and aerosol-cloud interaction (ACI) in January and July 2013

371 in eastern China, the error bars represent the standard deviations for different
372 meteorological factors and PM_{2.5} concentration induced by ARI and ACI in
373 January and July 2013 in eastern China.

374

375 **3.2 The shift of the PM_{2.5} enhancements induced by ARI and ACI**

376 As discussed in section 3.1, the enhanced PM_{2.5} concentrations induced by
377 ARI and ACI exhibit obvious spatial and seasonal variations in 2013. However,
378 due to the variations of meteorological background and the reduction of
379 anthropogenic emission from 2013 to 2021, their joint and individual impacts on
380 the ARI- and ACI-induced PM_{2.5} enhancements are still unclear. Fig. 2 shows the
381 ARI- and ACI-induced PM_{2.5} enhancements in the experiments of 13M13E,
382 21M13E and 21M21E in January and July.

383 As shown in Fig. 2, from 2013 to 2021, the PM_{2.5} concentration
384 enhancement induced by the ARI in January decreases by 75% (from 5.59 to 1.37
385 $\mu\text{g m}^{-3}$). Zhang et al. (2022) also found that the ARI effect over China weakens
386 during 2013–2017, and the ratio of PM_{2.5} enhancement to the ambient PM_{2.5}
387 concentration decreases from 5.40% to 3.30%. The decline of the PM_{2.5}
388 enhancement ratio (2.10%) is lower than that in this study (3.26%) due to the
389 continuous emission reduction after 2017. On the other hand, the ACI-induced
390 PM_{2.5} enhancement decreases by 51%, from 3.96 to 1.93 $\mu\text{g m}^{-3}$. With lower
391 percentage decrease in the PM_{2.5} enhancement, the ACI-induced PM_{2.5}
392 enhancement exceeds the ARI-induced PM_{2.5} enhancement in January 2021. In

393 July, both the ARI- and ACI-induced $PM_{2.5}$ enhancements show decreasing trends,
394 the percentage decreases of the ARI-induced (31%) and ACI-induced (34%)
395 $PM_{2.5}$ enhancements are very close.

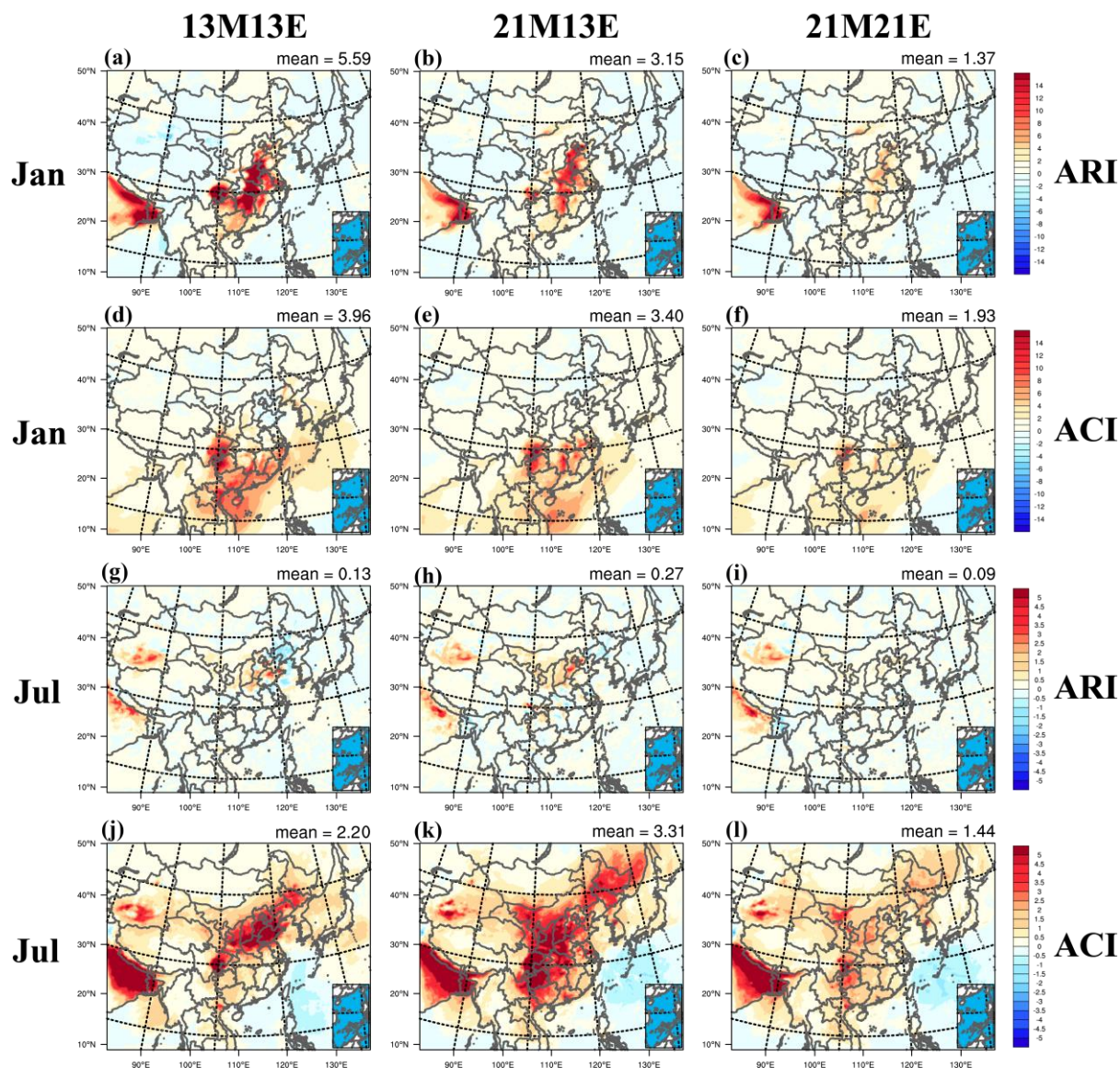
396 The contributions of the meteorological background variation and
397 anthropogenic emission reduction to the changes of the ARI- and ACI-induced
398 $PM_{2.5}$ enhancements are different. Due to the meteorological background change
399 from 2013 to 2021, the ARI- and ACI-induced $PM_{2.5}$ enhancements show
400 different characteristics in January and July. It can be seen that, the ARI-induced
401 $PM_{2.5}$ enhancement decreases from 5.59 to 3.15 $\mu g m^{-3}$ with the variation of
402 meteorological background in January, while it increases from 0.13 to 0.27 $\mu g m$
403 $^{-3}$ in July. The primary reason for the difference is that the ambient $PM_{2.5}$
404 concentration decreases in January but increases in July caused by different
405 meteorological backgrounds. The ACI-induced $PM_{2.5}$ enhancement changes
406 slightly from 3.96 to 3.40 $\mu g m^{-3}$ in January due to the variation of meteorological
407 background. However, it increases from 2.20 to 3.31 $\mu g m^{-3}$ in July, because of
408 a large aerosol-induced LWP increase in July 2021.

409 Considering the reduction of anthropogenic emission, the ARI- and ACI-
410 induced $PM_{2.5}$ enhancements both show declining trends (middle and right
411 columns in Fig. 2). The ARI-induced $PM_{2.5}$ enhancement decreases by 56.51% in
412 January, from 3.15 to 1.37 $\mu g m^{-3}$. The ACI-induced $PM_{2.5}$ enhancement
413 decreases by 43.24%, from 3.40 to 1.93 $\mu g m^{-3}$. The percentage decrease of the
414 ACI-induced $PM_{2.5}$ enhancement is lower than that of the ARI-induced in January,

415 which also occurs in July, when the ARI-induced $\text{PM}_{2.5}$ enhancement decreases
416 by 66.67% (from 0.27 to 0.09 $\mu\text{g m}^{-3}$) and ACI-induced $\text{PM}_{2.5}$ enhancement
417 decreases by 56.50% (from 3.31 to 1.44 $\mu\text{g m}^{-3}$).

418 In summary, both the variation of meteorological background and the
419 reduction of anthropogenic emission play important roles in changing the ARI-
420 and ACI-induced $\text{PM}_{2.5}$ enhancements. However, the decreases of ARI- and ACI-
421 induced $\text{PM}_{2.5}$ enhancements from 2013 to 2021 are primarily attributed to the
422 reduction of anthropogenic emission. In addition, the percentage decrease of the
423 ACI-induced $\text{PM}_{2.5}$ enhancement is lower than that induced by the ARI in both
424 January and July. Therefore, the ACI-induced $\text{PM}_{2.5}$ enhancement has become
425 increasingly important in both January and July from 2013 to 2021.

426



427

428 Fig. 2. The distributions of enhanced PM_{2.5} concentrations (unit: $\mu\text{g m}^{-3}$) induced

429 by the ARI (first and third rows) and the ACI (second and fourth rows) in January

430 (first and second rows) and July (third and fourth rows) in the experiments of

431 13M13E (left column), 21M13E (middle column) and 21M21E (right column).

432

433 3.3 The changes in the enhanced PM_{2.5} components induced by the

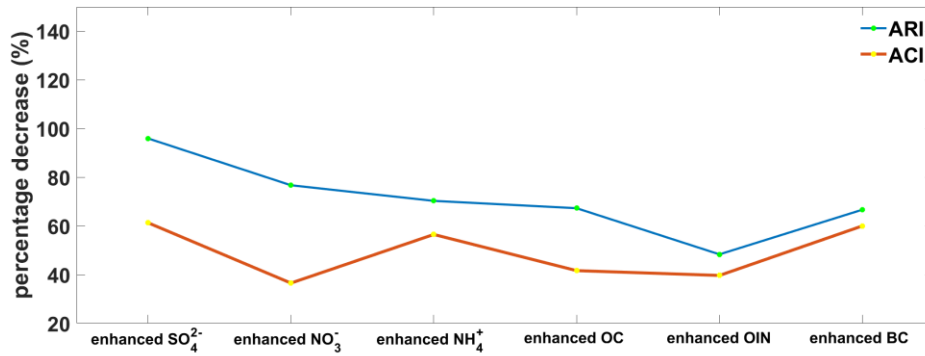
434 ARI and the ACI

435 In terms of the anthropogenic emission reduction, the percentage decrease

436 of the ACI-induced $PM_{2.5}$ enhancement is lower than that induced by the ARI in
437 both January and July. We find that the difference is primarily from the different
438 percentage decreases of the secondary $PM_{2.5}$ component enhancements induced
439 by ARI and ACI.

440 Fig. 3 shows the percentage decreases of ARI- and ACI-induced $PM_{2.5}$
441 component enhancements caused by the anthropogenic emission reduction in
442 January and July. It can be seen that the difference between the percentage
443 decreases of the ARI- and ACI-induced enhancements of sulfate, nitrate,
444 ammonium and OC is larger than those of BC and other inorganic aerosol (OIN).
445 OIN refers to inorganic compositions other than sulfate, nitrate, ammonium, and
446 BC. These compositions include sea salt and mineral elements. Specifically, the
447 difference between the percentage decreases for sulfate, nitrate, ammonium and
448 OC enhancements are 34.66%, 40.20%, 13.80% and 25.65% respectively, and the
449 values for OIN and BC are 8.67% and 6.67%. This result indicates that the lower
450 decrease in the ACI-induced $PM_{2.5}$ concentration enhancement is mainly due to
451 the small decrease in the ACI-induced enhancements of secondary $PM_{2.5}$
452 components. The main causes will be illustrated in section 3.4.

453



454

455 Fig. 3. Percentage decreases (21M13E–21M21E)/21M13E) of the spatial and
 456 temporal average ARI- and ACI-induced PM_{2.5} component enhancements in
 457 eastern China in January and July caused by the anthropogenic emission
 458 reduction from 2013 to 2021.

459

460 **3.4 Causes for the increased importance of ACI**

461 **3.4.1 Explanation from the perspective of meteorological changes**

462 As discussed in previous studies, the decrease of PBLH and T2 and the
 463 increase of RH are tightly related to the ARI- and ACI-induced PM_{2.5}
 464 enhancements (Donahue et al., 2012; Ding et al., 2016; Moch et al., 2022; Liu et
 465 al., 2018). From the perspective of the ARI- and ACI-induced changes in
 466 meteorological factors, we investigate the primary reasons for the increasing
 467 importance of the ACI-induced PM_{2.5} enhancement under the reduction of
 468 anthropogenic emission.

469 Fig. 4 shows the percentage decreases of ARI- and ACI-induced decrease of
 470 SWDOWN, PBLH and T2 and increase of RH due to the reduction of
 471 anthropogenic emission from 2013 to 2021. In January, in order to illustrate the

472 reasons of the lower percentage decrease in the ACI-induced $PM_{2.5}$ enhancement
473 clearly, we take the highly polluted NCP region as an example. As shown in Fig.
474 4c, the percentage decreases of the ACI-induced decline of SWDOWN (19%),
475 PBLH (27%) and T2 (20%) and the increase of RH (24%) are lower than those
476 of the ARI-induced decline of SWDOWN (29%), PBLH (39%) and T2 (32%) and
477 the increase of RH (36%). The phenomenon in July is similar with that in January
478 (Figs. 4a and b). To our knowledge, the PBLH and T2 are determined by the
479 incoming solar radiation at the surface, and they can strongly influence the RH.
480 So the lower percentage decrease in the ACI-induced reductions of PBLH and T2
481 and increase of RH could be explained by the lower percentage decrease in the
482 ACI-induced SWDOWN reduction.

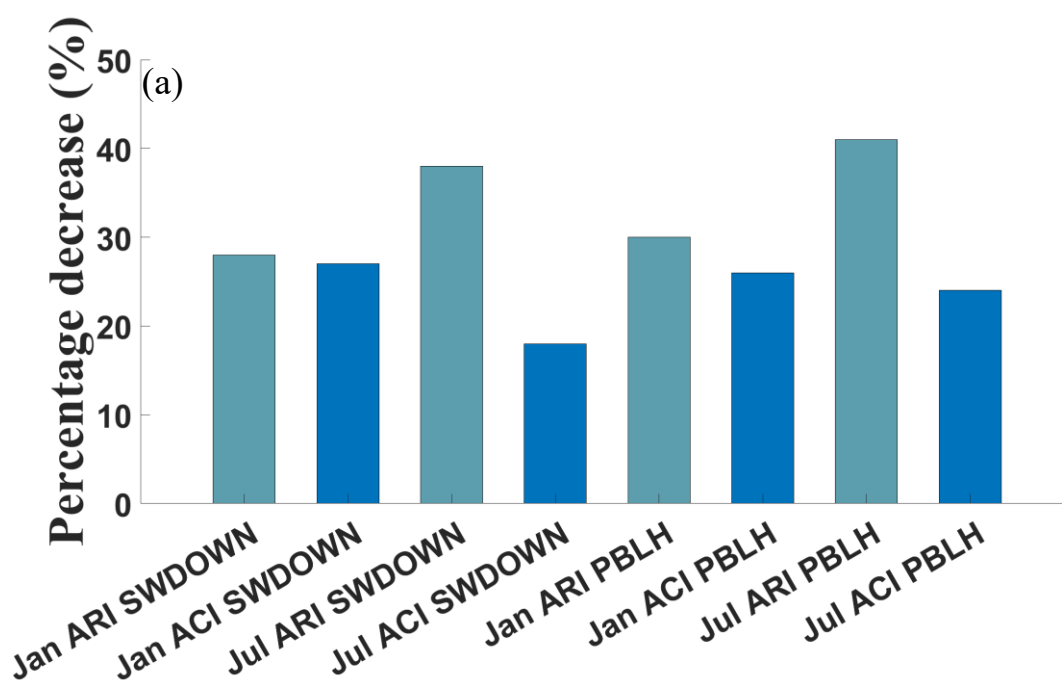
483 We believe that the relatively lower decrease in the ACI-induced SWDOWN
484 reduction is inevitable under high ambient $PM_{2.5}$ concentration. As shown in Fig.
485 S8b, the SWDOWN reduction induced by the ARI shows a linear relationship
486 with the decline of ambient $PM_{2.5}$ concentration, which is similar with Zhou et al.
487 (2018). In contrast, the decrease in the SWDOWN reduction induced by the ACI
488 is lower than that by the ARI due to the ambient $PM_{2.5}$ decrease in the high $PM_{2.5}$ -
489 polluted regime. The reason is that the decrease in ambient $PM_{2.5}$ concentration
490 directly weakens the ARI-induced SWDOWN reduction, but it has only a minor
491 impact on the ACI-induced SWDOWN reduction because the change in LWP and
492 cloud effective radius (Re) induced by ACI is not sensitive to $PM_{2.5}$ reduction in
493 the $PM_{2.5}$ -polluted regime. In our simulations, the influence of ACI-induced Re

494 change is relatively smaller than that of ACI-induced LWP change with a large
495 decrease in $PM_{2.5}$ concentration (Fig. S7). Therefore, we are only concerned with
496 change in ACI-induced LWP with a reduction in $PM_{2.5}$. As shown in Fig. S8a,
497 when the ambient $PM_{2.5}$ concentration exceeded $15 \mu\text{g m}^{-3}$, the decrease in ACI-
498 induced LWP increase is relatively low with a $PM_{2.5}$ reduction from 120 to $15 \mu\text{g}$
499 m^{-3} , indicating that aerosols are not a key limiting factor to cloud formation in
500 this range. Note that when the ambient $PM_{2.5}$ concentration decreases to $15 \mu\text{g}$
501 m^{-3} , the weakening of SWDOWN reduction induced by the ACI might be larger
502 than that by the ARI. This is because decrease in ACI-induced LWP increase is
503 relatively fast, with a $PM_{2.5}$ reduction from 15 to $0 \mu\text{g m}^{-3}$. Previous studies have
504 demonstrated that the decrease in ACI-induced LWP increase is relatively fast or
505 slow with the ambient $PM_{2.5}$ reduction in the $PM_{2.5}$ -clean or polluted condition,
506 respectively (Myhre et al., 2007; Savane et al., 2015). The regional and temporal
507 average $PM_{2.5}$ concentration in eastern China in January and July simulated using
508 background meteorology in 2021 and emissions in 2013 is 63 and $25 \mu\text{g m}^{-3}$,
509 which is much higher than $15 \mu\text{g m}^{-3}$. Therefore, the decrease in ACI-induced
510 SWDOWN reduction in both months is weak.

511 Especially, the lower PBLH caused by ARI and ACI will enhance the
512 accumulation of all the $PM_{2.5}$ components, but higher RH and lower T2 induced
513 by the ARI and ACI could promote the production of extra secondary $PM_{2.5}$
514 components through strengthening aqueous and heterogeneous reactions and
515 causing gas precursors to condense into particle matter (Donahue et al., 2012; Liu

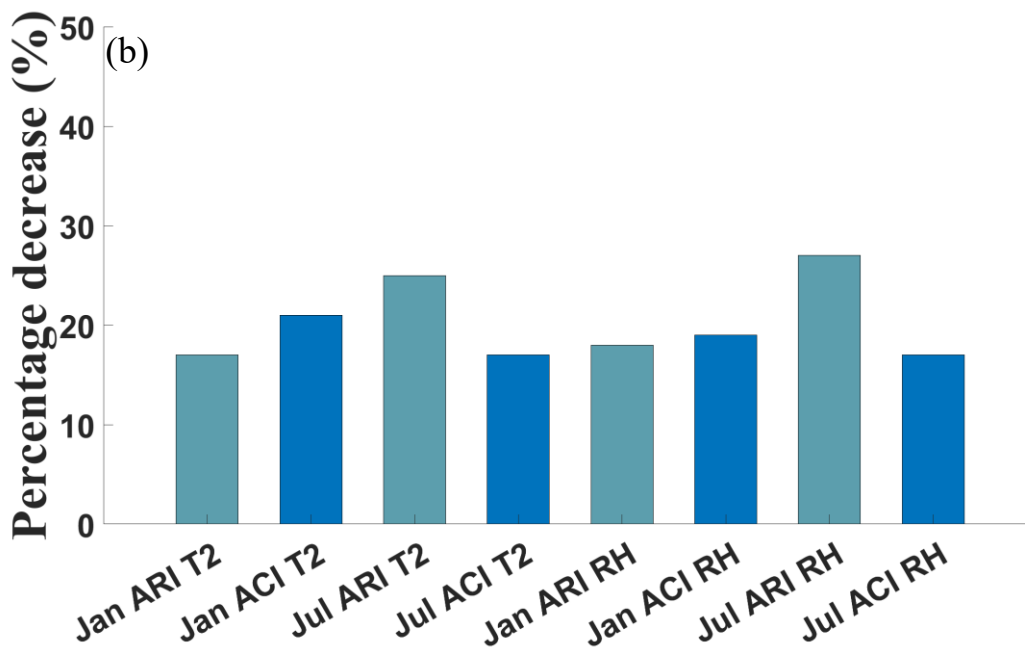
516 et al., 2018). Therefore, lower percentage decrease in the T2 reduction and RH
517 increase induced by the ACI is more likely to weaken the decrease in the
518 enhancements of secondary PM_{2.5} components. This well explains the lower
519 percentage decreases in the enhancements of secondary PM_{2.5} components
520 induced by the ACI than those by the ARI as shown in Fig. 3.

521



522

523



524



525

526 Fig. 4. The percentage decreases of the regional averages of (a) the decrease of
 527 SWDOWN and PBLH, and (b) the T2 reduction and RH increase induced by ARI
 528 and ACI in eastern China caused by the anthropogenic emission reduction in
 529 January and July from 2013 to 2021. (c) is the same as (a) and (b), but in the NCP
 530 region in January.

531

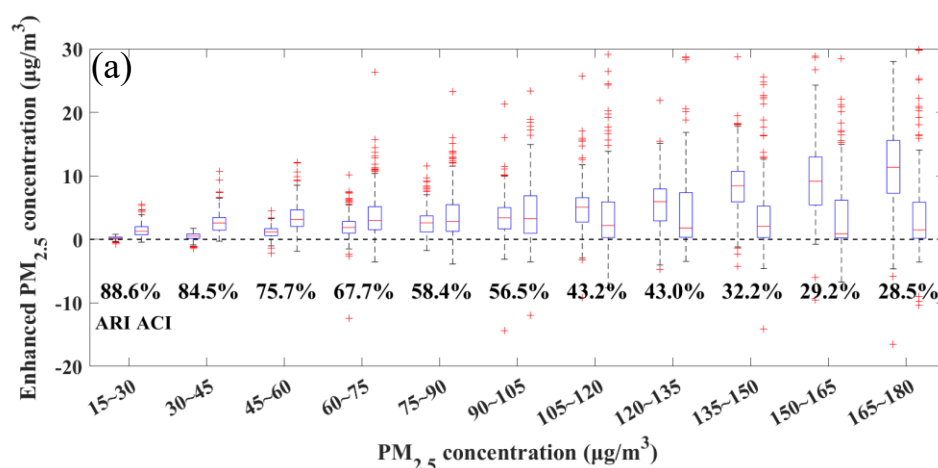
532 **3.4.2 Explanation from the perspective of PM_{2.5} concentration distribution** 533 **changes**

534 Ambient PM_{2.5} concentration is the fundamental factor to trigger the ARI
535 and the ACI. In order to further explore the reasons for the increasing importance
536 of enhanced PM_{2.5} concentration induced by ACI, we discuss the characteristics
537 of enhanced PM_{2.5} concentration induced by ARI and ACI under different PM_{2.5}
538 pollution levels. Given that this study mainly focuses on the change in ARI- and
539 ACI-induced PM_{2.5} enhancement in the PM_{2.5}-polluted regime, we only discuss
540 these changes within the PM_{2.5} concentration range of 15–180 $\mu\text{g m}^{-3}$

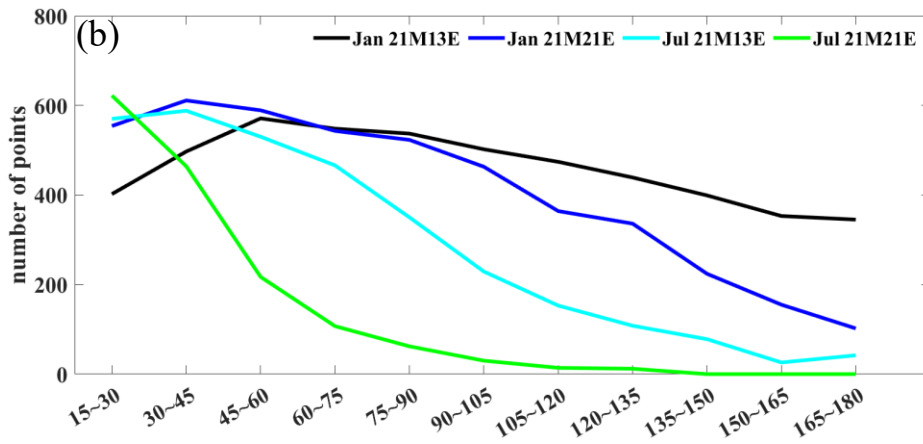
541 The PM_{2.5} concentration is divided into 11 levels from 15 to 180 $\mu\text{g m}^{-3}$. As
542 shown in Fig. 5a, in the heavily PM_{2.5}-polluted regime (135–180 $\mu\text{g m}^{-3}$), the
543 decrease in SWDOWN induced by ARI is much larger than that induced by ACI
544 (Fig. S9a). Then, the decrease in PBLH and T2 and the increase in RH induced
545 by ARI are also larger than those induced by ACI (Fig. S9b–d). Thus, the
546 enhanced PM_{2.5} induced by the ARI is much larger than that by the ACI (Fig. 5a).
547 However, when the PM_{2.5} concentration decrease to the range of 15–45 $\mu\text{g m}^{-3}$,
548 the decrease in SWDOWN, PBLH, and T2 and the increase in RH induced by
549 ACI significantly exceed those induced by ARI. Thus, the ACI-induced PM_{2.5}
550 enhancement significantly exceeds the ARI-induced PM_{2.5} enhancement and
551 becomes more important. This indicates the fast decrease in the ARI-induced
552 PM_{2.5} enhancement and the increasing contribution of the ACI-induced PM_{2.5}

553 enhancement with the decrease in the $PM_{2.5}$ concentration. In summary, the
 554 percentage decrease in the $PM_{2.5}$ enhancement induced by ACI is weaker than
 555 that induced by ARI with the decrease of $PM_{2.5}$ concentration because of the
 556 lower percentage decrease in the ACI-induced SWDOWN, which causes the
 557 lower percentage decrease in the ACI-induced PBLH and T2 reduction and the
 558 RH increase. Furthermore, as shown in Fig. S8a, the low percentage decrease in
 559 the ACI-induced SWDOWN reduction is due to a low decrease in the ACI-
 560 induced LWP in the $PM_{2.5}$ -polluted regime. Considering the decrease in the
 561 ambient $PM_{2.5}$ concentration due to the anthropogenic emission reduction from
 562 2013 to 2021 (Fig. 5b), the ACI-induced $PM_{2.5}$ enhancement certainly contributes
 563 more to the total $PM_{2.5}$ concentration in 2021.

564



565



566

567 Fig. 5. (a) The enhanced PM_{2.5} concentrations induced by ARI and ACI at
 568 different ambient PM_{2.5} levels. These data are from the simulations for January
 569 and July in the experiments of 21M13E and 21M21E. The percentage represents
 570 the ratio of the ACI-induced PM_{2.5} enhancement to the sum of ARI- and ACI-
 571 induced PM_{2.5} enhancements. (b) The distributions of ambient PM_{2.5} levels in
 572 January and July in the experiments of 21M13E and 21M21E.

573

574 4. Conclusions

575 Under the background of sharpened anthropogenic emission reduction, this
 576 study investigates changes of the ARI- and ACI-induced PM_{2.5} enhancements for
 577 2013–2021, and explores the causes for these changes from the perspectives of
 578 meteorological factors and PM_{2.5} concentration distribution.

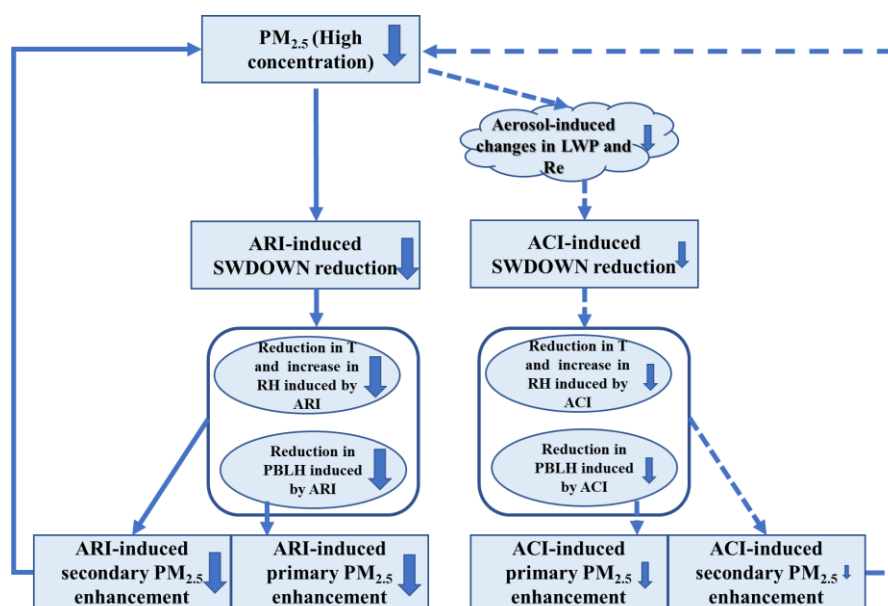
579 The results show that the enhanced PM_{2.5} induced by the ARI (5.59 μg m⁻³)
 580 is greater than that by the ACI (3.96 μg m⁻³) in January 2013. However, the ARI-
 581 and ACI-induced PM_{2.5} enhancements decrease from 5.59 and 3.96 μg m⁻³ to 1.37
 582 and 1.93 μg m⁻³ in January and decrease by 75% and 51% for 2013–2021. The

583 smaller decrease ratio (51%) for ACI-induced $PM_{2.5}$ enhancements implies that
584 ACI becomes more important for enhancing $PM_{2.5}$ concentrations in January
585 2021. Furthermore, we separated the contributions of meteorological background
586 variation and anthropogenic emission reduction. Compared with the
587 meteorological background variation, anthropogenic emission reduction plays a
588 more important role in causing the decrease of ARI- and ACI-induced $PM_{2.5}$
589 enhancements. Owing to only emission reduction, the enhanced $PM_{2.5}$
590 concentrations induced by the ARI and ACI decrease by 56% and 43% in January
591 and 66% and 56% in July, respectively. The ACI-induced $PM_{2.5}$ enhancement
592 becomes increasingly important in both January and July for 2013–2021. More
593 specifically, the lower percentage decrease in the ACI-induced $PM_{2.5}$
594 enhancement is dominated by the lower decrease in the enhancements of
595 secondary $PM_{2.5}$ components.

596 The lower percentage decrease in the enhanced $PM_{2.5}$ induced by the ACI is
597 due to the lower percentage decrease in the ACI-induced SWDOWN reduction,
598 which is because of the lower decrease in the LWP and increase in the Re caused
599 by the ambient $PM_{2.5}$ decrease in the high $PM_{2.5}$ -polluted regime (Fig. 6). At the
600 same time, the lower percentage decreases in the T2 reduction and RH increase
601 induced by the ACI further lead to the lower percentage decrease in the
602 enhancements of the ACI-induced secondary $PM_{2.5}$ components (Fig. 6). Notably,
603 due to relative lower percentage decrease in the ACI-induced SWDOWN
604 reduction in the high $PM_{2.5}$ -polluted regime, the increasing importance of ACI-

605 induced $PM_{2.5}$ enhancement is a matter of course with the ambient $PM_{2.5}$ decrease.

606



607

608 Fig. 6. Schematic diagram for the decrease of ARI- and ACI-induced primary and

609 secondary $PM_{2.5}$ enhancement due to reduction in ambient $PM_{2.5}$ concentration.

610 Solid arrows represent these processes are strongly weakened; dotted arrows

611 represent these processes are slightly weakened.

612

613 This study has important implication for the $PM_{2.5}$ control. As we know,

614 ARI- and ACI-induced $PM_{2.5}$ enhancements have a non-negligible contribution

615 to the deterioration of $PM_{2.5}$ air quality. Previous research has investigated the

616 impact of anthropogenic emission reduction on the ARI-induced $PM_{2.5}$

617 enhancement (Zhou et al., 2019). But compared with $PM_{2.5}$ enhancement induced

618 by ARI, that induced by ACI is more complicated and harder to be alleviated. Our

619 findings have further revealed that the ACI-induced $PM_{2.5}$ enhancement is getting

620 more important relative to that induced by ARI. This is especially true in cloud-

621 prone areas like Sichuan-Chongqing area, which have witnessed rather weak
622 decreases of ACI-induced $PM_{2.5}$ concentration in the past decade due to weak
623 decreases of aerosol-induced LWP under the condition of high ambient $PM_{2.5}$
624 level (Fig. 2). The ACI-induced $PM_{2.5}$ enhancement needs to be considered more
625 seriously in the formulation of control polices to meet national $PM_{2.5}$ air
626 quality standard, especially in cloud-prone areas with high ambient $PM_{2.5}$
627 concentration. To control ACI-induced $PM_{2.5}$ enhancement, first, a larger
628 emission reduction is necessary in cloudy areas compared with less cloudy areas
629 to bring about a noticeable decrease in ACI-induced LWP in response to $PM_{2.5}$
630 reduction. Second, secondary inorganic aerosol (SNA), which is an important
631 component of total aerosol, has a large influence on the ACI-induced $PM_{2.5}$
632 enhancement because of its high hygroscopicity. This makes it easy for SNA to
633 be activated as CCN and influence LWP. We think that it is crucial to make
634 substantial decreases in the precursors of SNA, such as SO_2 , NO_x and NH_3 species.
635 These decreases could substantially decrease SNA. A large decrease in SNA
636 would enhance the ACI-induced LWP response to $PM_{2.5}$ reduction and cause a
637 large decrease in ACI-induced $PM_{2.5}$ enhancement. In addition, relative to ARI-
638 induced $PM_{2.5}$ enhancement, the lower decrease in ACI-induced $PM_{2.5}$
639 enhancement is mainly because of the small decrease in ACI-induced
640 enhancements of secondary $PM_{2.5}$ components. A substantial decrease in SNA
641 would make the decrease ratio of ACI-induced $PM_{2.5}$ enhancement approach the
642 more rapid decrease ratio of ARI-induced $PM_{2.5}$ enhancement.

643

644 **Data and Code availability.**

645 The data and code used in this study are available upon request from Da Gao
646 (dagao94@foxmail.com).

647

648 **Author Contribution**

649 D.G., B.Z. and S.W. designed the research; D.G., B.Z., J.S. and B.G. improved
650 the WRF-Chem performance; D.G. and B.Z. further developed WRF-Chem and
651 performed the simulations; X.W., S.L. and Z.D. provide the anthropogenic
652 emissions; D.G. analyzed the data with the help from B.Z., S.W. and Y.W.; D.Y.
653 and J.S. help D.G. to design some figures; S.W., Y.W., Y.Z. and Y.H. presented
654 important suggestions for the analysis and writings; D.G. and B.Z. wrote the
655 paper with inputs from all co-authors.

656

657 **Competing interests**

658 The author declares no competing interests.

659

660 **Acknowledgments.**

661 This research is supported by the National Key Research and Development
662 Program of China (2022YFC3701000, Task 5), the National Natural Science
663 Foundation of China (22188102), and the Tencent Foundation through the
664 XPLORER PRIZE. We would like to thank Fenfen Zhang for providing the PM_{2.5}

665 components data for Handan city in January 2013.

666

667 **References**

668 Abdul-Razzak, H., and Ghan, S. J.: A parameterization of aerosol activation - 3.

669 Sectional representation, *J Geophys Res-Atmos*, 107, Artn 4026

670 10.1029/2001jd000483, 2002.

671 Bellouin, N., Quaas, J., Gryspeerdt, E., Kinne, S., Stier, P., Watson-Parris, D.,

672 Boucher, O., Carslaw, K. S., Christensen, M., Daniau, A. L., Dufresne, J. L.,

673 Feingold, G., Fiedler, S., Forster, P., Gettelman, A., Haywood, J. M.,

674 Lohmann, U., Malavelle, F., Mauritsen, T., McCoy, D. T., Myhre, G.,

675 Mulmenstadt, J., Neubauer, D., Possner, A., Rugenstein, M., Sato, Y., Schulz,

676 M., Schwartz, S. E., Sourdeval, O., Storelvmo, T., Toll, V., Winker, D., and

677 Stevens, B.: Bounding Global Aerosol Radiative Forcing of Climate Change,

678 *Rev Geophys*, 58, ARTN e2019RG000660 10.1029/2019RG000660, 2020.

679 Bennartz, R.: Global assessment of marine boundary layer cloud droplet number

680 concentration from satellite, *J Geophys Res-Atmos*, 112, Artn D02201

681 10.1029/2006jd007547, 2007.

682 Bougeault, P., and Lacarrere, P.: Parameterization Of Orography-Induced

683 Turbulence In a Mesobeta-Scale Model, *Mon Weather Rev*, 117, 1872-1890,

684 Doi 10.1175/1520-0493(1989)117<1872:Pooiti>2.0.Co;2, 1989.

685 Carter, W.: Documentation of the SAPRC-99 Chemical Mechanism for VOC

686 Reactivity Assessment, 2000.

687 Ding, A. J., Huang, X., Nie, W., Sun, J. N., Kerminen, V. M., Petaja, T., Su, H.,
688 Cheng, Y. F., Yang, X. Q., Wang, M. H., Chi, X. G., Wang, J. P., Virkkula,
689 A., Guo, W. D., Yuan, J., Wang, S. Y., Zhang, R. J., Wu, Y. F., Song, Y., Zhu,
690 T., Zilitinkevich, S., Kulmala, M., and Fu, C. B.: Enhanced haze pollution
691 by black carbon in megacities in China, *Geophys Res Lett*, 43, 2873-2879,
692 10.1002/2016GL067745, 2016.

693 Ding, D., Xing, J., Wang, S. X., Liu, K. Y., and Hao, J. M.: Estimated
694 Contributions of Emissions Controls, Meteorological Factors, Population
695 Growth, and Changes in Baseline Mortality to Reductions in Ambient
696 PM_{2.5} and PM_{2.5}-Related Mortality in China, 2013-2017, *Environ Health*
697 *Persp*, 127, Artn 067009 10.1289/Ehp4157, 2019.

698 Donahue, N. M., Henry, K. M., Mentel, T. F., Kiendler-Scharr, A., Spindler, C.,
699 Bohn, B., Brauers, T., Dorn, H. P., Fuchs, H., Tillmann, R., Wahner, A.,
700 Saathoff, H., Naumann, K. H., Mohler, O., Leisner, T., Muller, L., Reinnig,
701 M. C., Hoffmann, T., Salo, K., Hallquist, M., Frosch, M., Bilde, M., Tritscher,
702 T., Barmet, P., Praplan, A. P., DeCarlo, P. F., Dommen, J., Prevot, A. S. H.,
703 and Baltensperger, U.: Aging of biogenic secondary organic aerosol via gas-
704 phase OH radical reactions, *P Natl Acad Sci USA*, 109, 13503-13508,
705 10.1073/pnas.1115186109, 2012.

706 Emery, C., Tai, E., Yarwood, G. : Enhanced meteorological modeling and
707 performance evaluation for two texas episodes, Report to the Texas Natural
708 Resources Conservation Commission, 2001.

709 Fan, J. W., Wang, Y., Rosenfeld, D., and Liu, X. H.: Review of Aerosol-Cloud
710 Interactions: Mechanisms, Significance, and Challenges, *J Atmos Sci*, 73,
711 4221-4252, 10.1175/Jas-D-16-0037.1, 2016.

712 Fast, J. D., Gustafson, W. I., Easter, R. C., Zaveri, R. A., Barnard, J. C., Chapman,
713 E. G., Grell, G. A., and Peckham, S. E.: Evolution of ozone, particulates, and
714 aerosol direct radiative forcing in the vicinity of Houston using a fully
715 coupled meteorology-chemistry-aerosol model, *J Geophys Res-Atmos*, 111,
716 Artn D21305 10.1029/2005jd006721, 2006.

717 Forkel, R., Werhahn, J., Hansen, A. B., McKeen, S., Peckham, S., Grell, G., and
718 Suppan, P.: Effect of aerosol-radiation feedback on regional air quality - A
719 case study with WRF/Chem, *Atmos Environ*, 53, 202-211,
720 10.1016/j.atmosenv.2011.10.009, 2012.

721 Forkel, R., Balzarini, A., Baro, R., Bianconi, R., Curci, G., Jimenez-Guerrero, P.,
722 Hirtl, M., Honzak, L., Lorenz, C., Im, U., Perez, J. L., Pirovano, G., San Jose,
723 R., Tuccella, P., Werhahn, J., and Zabkar, R.: Analysis of the WRF-Chem
724 contributions to AQMEII phase2 with respect to aerosol radiative feedbacks
725 on meteorology and pollutant distributions, *Atmos Environ*, 115, 630-645,
726 10.1016/j.atmosenv.2014.10.056, 2015.

727 Forster, P., T. Storelvmo, K. Armour, W. Collins, J.-L. Dufresne, D. Frame, D.J.
728 Lunt, T. Mauritsen, M.D. Palmer, M. Watanabe, M. Wild, and H. Zhang: The
729 Earth's Energy Budget, Climate Feedbacks, and Climate Sensitivity. In
730 *Climate Change 2021: The Physical Science Basis. Contribution of Working*

731 Group I to the Sixth Assessment Report of the Intergovernmental Panel on
732 Climate Change [Masson-Delmotte, V., P. Zhai, A. Pirani, S.L. Connors, C.
733 Péan, S. Berger, N. Caud, Y. Chen, L. Goldfarb, M.I. Gomis, M. Huang,
734 K. Leitzell, E. Lonnoy, J.B.R. Matthews, T.K. Maycock, T. Waterfield, O.
735 Yelekçi, R. Yu, and B. Zhou (eds.)], Cambridge, United Kingdom and New
736 York, NY, USA, Cambridge University Press, 923–1054, 2021.

737 Gao, M., Han, Z. W., Tao, Z. N., Li, J. W., Kang, J. E., Huang, K., Dong, X. Y.,
738 Zhuang, B. L., Li, S., Ge, B. Z., Wu, Q. Z., Lee, H. J., Kim, C. H., Fu, J. S.,
739 Wang, T. J., Chin, M., Li, M., Woo, J. H., Zhang, Q., Cheng, Y. F., Wang, Z.
740 F., and Carmichael, G. R.: Air quality and climate change, Topic 3 of the
741 Model Inter-Comparison Study for Asia Phase III (MICS-Asia III) - Part 2:
742 aerosol radiative effects and aerosol feedbacks, *Atmos Chem Phys*, 20,
743 1147-1161, 10.5194/acp-20-1147-2020, 2020.

744 Gong, W., Makar, P. A., Zhang, J., Milbrandt, J., Gravel, S., Hayden, K. L.,
745 Macdonald, A. M., and Leitch, W. R.: Modelling aerosol-cloud-
746 meteorology interaction: A case study with a fully coupled air quality model
747 (GEM-MACH), *Atmos Environ*, 115, 695-715,
748 10.1016/j.atmosenv.2015.05.062, 2015.

749 Grell, G. A., and Freitas, S. R.: A scale and aerosol aware stochastic convective
750 parameterization for weather and air quality modeling, *Atmos Chem Phys*,
751 14, 5233-5250, 10.5194/acp-14-5233-2014, 2014.

752 Guenther, A., Karl, T., Harley, P., Wiedinmyer, C., Palmer, P. I., and Geron, C.:

753 Estimates of global terrestrial isoprene emissions using MEGAN (Model of
754 Emissions of Gases and Aerosols from Nature), *Atmos Chem Phys*, 6, 3181-
755 3210, DOI 10.5194/acp-6-3181-2006, 2006.

756 Gustafson, W. I., Chapman, E. G., Ghan, S. J., Easter, R. C., and Fast, J. D.:
757 Impact on modeled cloud characteristics due to simplified treatment of
758 uniform cloud condensation nuclei during NEAQS 2004, *Geophys Res Lett*,
759 34, Artn L19809 10.1029/2007gl030021, 2007.

760 Hong, C. P., Zhang, Q., Zhang, Y., Davis, S. J., Zhang, X., Tong, D., Guan, D. B.,
761 Liu, Z., and He, K. B.: Weakening aerosol direct radiative effects mitigate
762 climate penalty on Chinese air quality, *Nat Clim Change*, 10, 845-+,
763 10.1038/s41558-020-0840-y, 2020.

764 Iacono, M. J., Delamere, J. S., Mlawer, E. J., Shephard, M. W., Clough, S. A., and
765 Collins, W. D.: Radiative forcing by long-lived greenhouse gases:
766 Calculations with the AER radiative transfer models, *J Geophys Res-Atmos*,
767 113, Artn D13103 10.1029/2008jd009944, 2008.

768 Janjic, Z. I.: The Step-Mountain Eta Coordinate Model - Further Developments
769 Of the Convection, Viscous Sublayer, And Turbulence Closure Schemes,
770 *Mon Weather Rev*, 122, 927-945, Doi 10.1175/1520-
771 0493(1994)122<0927:Tsmecm>2.0.Co;2, 1994.

772 Kanji, Z. A., Ladino, L. A., Wex, H., Boose, Y., Burkert-Kohn, M., Cziczo, D. J.,
773 and Kramer, M.: Overview of Ice Nucleating Particles, *Meteor Mon*, 58,
774 10.1175/Amsmonographs-D-16-0006.1, 2017.

775 Kong, X., Forkel, R., Sokhi, R. S., Suppan, P., Baklanov, A., Gauss, M., Brunner,
776 D., Baro, R., Balzarini, A., Chemel, C., Curci, G., Jimenez-Guerrero, P.,
777 Hirtl, M., Honzak, L., Im, U., Perez, J. L., Pirovano, G., San Jose, R.,
778 Schlunzen, K. H., Tsegas, G., Tuccella, P., Werhahn, J., Zabkar, R., and
779 Galmarini, S.: Analysis of meteorology-chemistry interactions during air
780 pollution episodes using online coupled models within AQMEII phase-2,
781 *Atmos Environ*, 115, 527-540, 10.1016/j.atmosenv.2014.09.020, 2015.

782 Le, T. H., Wang, Y., Liu, L., Yang, J. N., Yung, Y. L., Li, G. H., and Seinfeld, J.
783 H.: Unexpected air pollution with marked emission reductions during the
784 COVID-19 outbreak in China, *Science*, 369, 702-+,
785 10.1126/science.abb7431, 2020.

786 Li, L., An, J. Y., Zhou, M., Yan, R. S., Huang, C., Lu, Q., Lin, L., Wang, Y. J., Tao,
787 S. K., Qiao, L. P., Zhu, S. H., and Chen, C. H.: Source apportionment of fine
788 particles and its chemical components over the Yangtze River Delta, China
789 during a heavy haze pollution episode, *Atmos Environ*, 123, 415-429,
790 10.1016/j.atmosenv.2015.06.051, 2015.

791 Li, M., Zhang, Q., Kurokawa, J., Woo, J. H., He, K. B., Lu, Z. F., Ohara, T., Song,
792 Y., Streets, D. G., Carmichael, G. R., Cheng, Y. F., Hong, C. P., Huo, H.,
793 Jiang, X. J., Kang, S. C., Liu, F., Su, H., and Zheng, B.: MIX: a mosaic Asian
794 anthropogenic emission inventory under the international collaboration
795 framework of the MICS-Asia and HTAP, *Atmos Chem Phys*, 17, 935-963,
796 10.5194/acp-17-935-2017, 2017.

797 Li Shengyue, W. S., Wu Qingru: Emission trends of air pollutants and CO₂ in
798 China from 2005 to 2021, Earth System Science Data,
799 <https://doi.org/10.5194/essd-2022-464>, 2023.

800 Lin, C. J.: Characteristics and Sources of Water-soluble Inorganic Ions in
801 Atmospheric Particulate Matter and Rainfall in the suburb of Mianyang,
802 Master, Southwest University of Science and Technology, 2022.

803 Liu, Q., Jia, X. C., Quan, J. N., Li, J. Y., Li, X., Wu, Y. X., Chen, D., Wang, Z. F.,
804 and Liu, Y. G.: New positive feedback mechanism between boundary layer
805 meteorology and secondary aerosol formation during severe haze events, Sci
806 Rep-Uk, 8, Artn 6095 10.1038/S41598-018-24366-3, 2018.

807 Liu, Y. Y., Xing, J., Wang, S. X., Fu, X., and Zheng, H. T.: Source-specific
808 speciation profiles of PM_{2.5} for heavy metals and their anthropogenic
809 emissions in China, Environ Pollut, 239, 544-553,
810 10.1016/j.envpol.2018.04.047, 2018.

811 Liu, S., Xing, J., Zhao, B., Wang, J. D., Wang, S. X., Zhang, X. Y., and Ding, A.
812 J.: Understanding of Aerosol-Climate Interactions in China: Aerosol Impacts
813 on Solar Radiation, Temperature, Cloud, and Precipitation and Its Changes
814 Under Future Climate and Emission Scenarios, Curr Pollut Rep, 5, 36-51,
815 10.1007/s40726-019-00107-6, 2019.

816 Matthias, V., Aulinger, A., Bieser, J., Chen, Y. J., Geyer, B., Gao, J., Quante, M.,
817 and Zhang, F.: Modeling high aerosol loads in China in January 2013, Urban
818 Clim, 22, 35-50, 10.1016/j.uclim.2016.04.005, 2017.

819 Moch, J. M., Mickley, L. J., Keller, C. A., Bian, H. S., Lundgren, E. W., Zhai, S.
820 X., and Jacob, D. J.: Aerosol-Radiation Interactions in China in Winter:
821 Competing Effects of Reduced Shortwave Radiation and Cloud-Snowfall-
822 Albedo Feedbacks Under Rapidly Changing Emissions, *J Geophys Res-*
823 *Atmos*, 127, ARTN e2021JD035442 10.1029/2021JD035442, 2022.

824 Morrison, H., Thompson, G., and Tatarskii, V.: Impact of Cloud Microphysics on
825 the Development of Trailing Stratiform Precipitation in a Simulated Squall
826 Line: Comparison of One- and Two-Moment Schemes, *Mon Weather Rev*,
827 137, 991-1007, 10.1175/2008MWR2556.1, 2009.

828 Myhre, G., Stordal, F., Johnsrud, M., Kaufman, Y. J., Rosenfeld, D., Storelvmo,
829 T., Kristjansson, J. E., Berntsen, T. K., Myhre, A., and Isaksen, I. S. A.:
830 Aerosol-cloud interaction inferred from MODIS satellite data and global
831 aerosol models, *Atmos Chem Phys*, 7, 3081-3101, DOI 10.5194/acp-7-
832 3081-2007, 2007.

833 Niu, G. Y., Yang, Z. L., Mitchell, K. E., Chen, F., Ek, M. B., Barlage, M., Kumar,
834 A., Manning, K., Niyogi, D., Rosero, E., Tewari, M., and Xia, Y. L.: The
835 community Noah land surface model with multiparameterization options
836 (Noah-MP): 1. Model description and evaluation with local-scale
837 measurements, *J Geophys Res-Atmos*, 116, Artn D12109
838 10.1029/2010jd015139, 2011.

839 Rosenfeld, D., Sherwood, S., Wood, R., and Donner, L.: Climate Effects of
840 Aerosol-Cloud Interactions, *Science*, 343, 379-380,

841 10.1126/science.1247490, 2014.

842 Savane, O. S., Vant-Hull, B., Mahani, S., and Khanbilvardi, R.: Effects of Aerosol
843 on Cloud Liquid Water Path: Statistical Method a Potential Source for
844 Divergence in Past Observation Based Correlative Studies, *Atmosphere-*
845 *Basel*, 6, 273-298, 10.3390/atmos6030273, 2015.

846 Seinfeld, J. H., Bretherton, C., Carslaw, K. S., Coe, H., DeMott, P. J., Dunlea, E.
847 J., Feingold, G., Ghan, S., Guenther, A. B., Kahn, R., Kraucunas, I.,
848 Kreidenweis, S. M., Molina, M. J., Nenes, A., Penner, J. E., Prather, K. A.,
849 Ramanathan, V., Ramaswamy, V., Rasch, P. J., Ravishankara, A. R.,
850 Rosenfeld, D., Stephens, G., and Wood, R.: Improving our fundamental
851 understanding of the role of aerosol-cloud interactions in the climate system,
852 *P Natl Acad Sci USA*, 113, 5781-5790, 10.1073/pnas.1514043113, 2016.

853 Shrivastava, M., Fast, J., Easter, R., Gustafson, W. I., Zaveri, R. A., Jimenez, J.
854 L., Saide, P., and Hodzic, A.: Modeling organic aerosols in a megacity:
855 comparison of simple and complex representations of the volatility basis set
856 approach, *Atmos Chem Phys*, 11, 6639-6662, 10.5194/acp-11-6639-2011,
857 2011.

858 Wang, J. D., Wang, S. X., Jiang, J. K., Ding, A. J., Zheng, M., Zhao, B., Wong,
859 D. C., Zhou, W., Zheng, G. J., Wang, L., Pleim, J. E., and Hao, J. M.: Impact
860 of aerosol-meteorology interactions on fine particle pollution during China's
861 severe haze episode in January 2013, *Environ Res Lett*, 9, Artn 094002
862 10.1088/1748-9326/9/9/094002, 2014.

863 Wang, Z. F., Li, J., Wang, Z., Yang, W., Tang, X., Ge, B., Yan, P., Zhu, L., Chen,
864 X., and Chen, H.: Modeling study of regional severe hazes over mid-eastern
865 China in January 2013 and its implications on pollution prevention and
866 control, *Science China Earth Sciences*, 3-13,
867 <https://doi.org/10.1007/s11430-013-4793-0>, 2014.

868 Wang, H., Shi, G. Y., Zhang, X. Y., Gong, S. L., Tan, S. C., Chen, B., Che, H. Z.,
869 and Li, T.: Mesoscale modelling study of the interactions between aerosols
870 and PBL meteorology during a haze episode in China Jing-Jin-Ji and its near
871 surrounding region - Part 2: Aerosols' radiative feedback effects, *Atmos*
872 *Chem Phys*, 15, 3277-3287, 10.5194/acp-15-3277-2015, 2015.

873 Wang, L. W., Wen, L., Xu, C. H., Chen, J. M., Wang, X. F., Yang, L. X., Wang,
874 W. X., Yang, X., Sui, X., Yao, L., and Zhang, Q. Z.: HONO and its potential
875 source particulate nitrite at an urban site in North China during the cold
876 season, *Sci Total Environ*, 538, 93-101, 10.1016/j.scitotenv.2015.08.032,
877 2015.

878 Wang, J. D., Zhao, B., Wang, S. X., Yang, F. M., Xing, J., Morawska, L., Ding,
879 A. J., Kulmala, M., Kerminen, V. M., Kujansuu, J., Wang, Z. F., Ding, D. A.,
880 Zhang, X. Y., Wang, H. B., Tian, M., Petaja, T., Jiang, J. K., and Hao, J. M.:
881 Particulate matter pollution over China and the effects of control policies,
882 *Sci Total Environ*, 584, 426-447, 10.1016/j.scitotenv.2017.01.027, 2017.

883 Wang, Y. S., Li, W. J., Gao, W. K., Liu, Z. R., Tian, S. L., Shen, R. R., Ji, D. S.,
884 Wang, S., Wang, L. L., Tang, G. Q., Song, T., Cheng, M. T., Wang, G. H.,

885 Gong, Z. Y., Hao, J. M., and Zhang, Y. H.: Trends in particulate matter and
886 its chemical compositions in China from 2013-2017, *Sci China Earth Sci*,
887 62, 1857-1871, 10.1007/s11430-018-9373-1, 2019.

888 Wild, O., Zhu, X., and Prather, M. J.: Fast-j: Accurate simulation of in- and
889 below-cloud photolysis in tropospheric chemical models, *J Atmos Chem*, 37,
890 245-282, Doi 10.1023/A:1006415919030, 2000.

891 Wu, J. R., Bei, N. F., Hu, B., Liu, S. X., Wang, Y., Shen, Z. X., Li, X., Liu, L.,
892 Wang, R. N., Liu, Z. R., Cao, J. J., Tie, X. X., Molina, L. T., and Li, G. H.:
893 Aerosol-photolysis interaction reduces particulate matter during wintertime
894 haze events, *P Natl Acad Sci USA*, 117, 9755-9761,
895 10.1073/pnas.1916775117, 2020.

896 Xiong, C. R., Li, J., Liu, Z. X., and Zhang, Z. Y.: The dominant role of aerosol-
897 cloud interactions in aerosol-boundary layer feedback: Case studies in three
898 megacities in China, *Front Env Sci-Switz*, 10, Artn 1002412
899 10.3389/Fenvs.2022.1002412, 2022.

900 Xue, C. Y., Zhang, C. L., Ye, C., Liu, P. F., Catoire, V., Krysztofiak, G., Chen, H.,
901 Ren, Y. G., Zhao, X. X., Wang, J. H., Zhang, F., Zhang, C. X., Zhang, J. W.,
902 An, J. L., Wang, T., Chen, J. M., Kleffmann, J., Mellouki, A., and Mu, Y. J.:
903 HONO Budget and Its Role in Nitrate Formation in the Rural North China
904 Plain, *Environ Sci Technol*, 54, 11048-11057, 10.1021/acs.est.0c01832,
905 2020.

906 Zaveri, R. A., Easter, R. C., Fast, J. D., and Peters, L. K.: Model for Simulating

907 Aerosol Interactions and Chemistry (MOSAIC), *J Geophys Res-Atmos*, 113,
908 Artn D13204 10.1029/2007jd008782, 2008.

909 Zhang, B., Wang, Y., and Hao, J.: Simulating aerosol-radiation-cloud feedbacks
910 on meteorology and air quality over eastern China under severe haze
911 conditions in winter, *Atmos Chem Phys*, 15, 2387-2404, 10.5194/acp-15-
912 2387-2015, 2015.

913 Zhang, F. F.: Characteristics of Air Pollution and Chemical Composition of
914 PM_{2.5} in Handan Master, College of Urban Construction, Hebei University
915 of Engineering, 2015.

916 Zhang, X., Zhang, Q., Hong, C. P., Zheng, Y. X., Geng, G. N., Tong, D., Zhang,
917 Y. X., and Zhang, X. Y.: Enhancement of PM_{2.5} Concentrations by Aerosol-
918 Meteorology Interactions Over China, *J Geophys Res-Atmos*, 123, 1179-
919 1194, 10.1002/2017JD027524, 2018.

920 Zhang, F., Wang, Y., Peng, J. F., Chen, L., Sun, Y. L., Duan, L., Ge, X. L., Li, Y.
921 X., Zhao, J. Y., Liu, C., Zhang, X. C., Zhang, G., Pan, Y. P., Wang, Y. S.,
922 Zhang, A. L., Ji, Y. M., Wang, G. H., Hu, M., Molina, M. J., and Zhang, R.
923 Y.: An unexpected catalyst dominates formation and radiative forcing of
924 regional haze, *P Natl Acad Sci USA*, 117, 3960-3966,
925 10.1073/pnas.1919343117, 2020.

926 Zhang, F. F., Xing, J., Ding, D. A., Wang, J. D., Zheng, H. T., Zhao, B., Qi, L.,
927 and Wang, S. X.: Role of black carbon in modulating aerosol direct effects
928 driven by air pollution controls during 2013-2017 in China, *Sci Total*

929 Environ, 832, ARTN 154928 10.1016/j.scitotenv.2022.154928, 2022.

930 Zhao, C., Liu, X., Leung, L. R., Johnson, B., McFarlane, S. A., Gustafson, W. I.,
931 Fast, J. D., and Easter, R.: The spatial distribution of mineral dust and its
932 shortwave radiative forcing over North Africa: modeling sensitivities to dust
933 emissions and aerosol size treatments, Atmos Chem Phys, 10, 8821-8838,
934 10.5194/acp-10-8821-2010, 2010.

935 Zhao, C., Chen, S., Leung, L. R., Qian, Y., Kok, J. F., Zaveri, R. A., and Huang,
936 J.: Uncertainty in modeling dust mass balance and radiative forcing from
937 size parameterization, Atmos Chem Phys, 13, 10733-10753, 10.5194/acp-
938 13-10733-2013, 2013.

939 Zhao, B., Liou, K. N., Gu, Y., Li, Q. B., Jiang, J. H., Su, H., He, C. L., Tseng, H.
940 L. R., Wang, S. X., Liu, R., Qi, L., Lee, W. L., and Hao, J. M.: Enhanced
941 PM_{2.5} pollution in China due to aerosol-cloud interactions, Sci Rep-Uk, 7,
942 Artn 4453 10.1038/S41598-017-04096-8, 2017.

943 Zheng, H. T., Cai, S. Y., Wang, S. X., Zhao, B., Chang, X., and Hao, J. M.:
944 Development of a unit-based industrial emission inventory in the Beijing-
945 Tianjin-Hebei region and resulting improvement in air quality modeling,
946 Atmos Chem Phys, 19, 3447-3462, 10.5194/acp-19-3447-2019, 2019.

947 Zhou, M., Zhang, L., Chen, D., Gu, Y., Fu, T. M., Gao, M., Zhao, Y. H., Lu, X.,
948 and Zhao, B.: The impact of aerosol-radiation interactions on the
949 effectiveness of emission control measures, Environ Res Lett, 14, Artn
950 024002 10.1088/1748-9326/Aaf27d, 2019.